Structures and properties of ferromagnetically coupled bis(μ-halo)diiron(II) complexes

Yan Zang, Ho G. Jang, Yu-Min Chiou, Michael P. Hendrich and Lawrence Que, Jr.*

Department of Chemistry, University of Minnesota, Minneapolis, MN 55455 (USA)

(Received March 2, 1993)

Abstract

Three bis(μ-halo)diferrous complexes, $[Fe_2(TLA)_2F_2](BF_4)_2$ (**1**), $[Fe_2(TMPzA)_2Cl_2](BPh_4)_2$ (**2**) and $[Fe_2(TPA)_2Cl_2](BPh_4)_2$ (**3**), have been synthesized and crystallographically characterized. The crystallographic data are as follows: **1**, triclinic system, space group $P\bar{1}$ (No. 2), with cell dimensions $a = 8.746(7)$, $b = 11.386(4)$, $c = 12.018(6)$ Å, $\alpha = 64.44(3)$, $\beta = 81.54(5)$, $\gamma = 87.90(5)°$, $V = 1067(2)$ Å^3, $R = 0.046$, $R_w = 0.063$; **2**, triclinic system, space group $P\bar{1}$ (No. 2), with cell dimensions $a = 10.440(5)$, $b = 11.610(8)$, $c = 16.98(1)$ Å, $\alpha = 77.55(6)$, $\beta = 79.63(5)$, $\gamma = 88.90(5)°$, $V = 1977(4)$ Å^3, $R = 0.042$, $R_w = 0.050$; **3**, monoclinic system, space group $C2/c$ (No. 15), with cell dimensions $a = 19.211(6)$, $b = 15.264(9)$, $c = 24.52(2)$ Å, $\beta = 105.57(3)°$, $V = 6926(4)$ Å^3, $R = 0.049$, $R_w = 0.053$. All three complexes have Fe_2X_2 cores with Fe–Fe distances of 3.198(3) Å for **1**, 3.563(3) Å for **2** and 3.494(3) Å for **3**, and Fe–X–Fe angles of 101.72(9)° for **1**, 91.94(6)° for **2** and 90.67(3)° for **3**. Magnetization studies over the temperature range of 2 to 200 K indicate that the high spin ferrous centers are ferromagnetically coupled in all three complexes. The parameter sets of the best fit ($H_{ex} = JS_1 \cdot S_2$) are for **1**: $J = -1.2(2)$ cm^{-1}, $|D_i| = 7.2(5)$ cm^{-1}, $g_i = 2.12(3)$; for **2**: $J = -2.6(2)$ cm^{-1}, $|D_i| = 7.2(5)$ cm^{-1}, $g_i = 2.15(3)$; and for **3**: $J = -10.0(2)$ cm^{-1}, $|D_i| = 13.2(5)$ cm^{-1}, $g_i = 2.15(3)$. The EPR signals near $g = 18$ also indicate ferromagnetic coupling between the iron(II) centers.

Introduction

The diferrous oxidation state plays an important role in the dioxygen chemistry of hemerythrin (Hr) [1], the R2 protein of ribonucleotide reductase (RNR) [2] and methane monooxygenase (MMO) [3], which constitute a new subclass of metalloproteins with non-heme diiron sites [4]. As a result of this development, a number of diiron(II) complexes have been synthesized to model these protein sites. The (μ-hydroxo)bis(μ-carboxylato-O,O') core found for deoxyHr [1] is represented by $[Fe_2(\mu\text{-OH})(\mu\text{-OAc})_2(Me_3TACN)_2]X$ [5]**, while the putative (μ-aqua)bis(μ-carboxylato-O,O') core of

deoxyHrN$_3$ [6] is mimicked by $[Fe_2(\mu\text{-}H_2O)(OAc)_4(tmen)_2]$ with terminal acetates stabilizing the aqua bridge by hydrogen bonding [7]. The use of the BIPhMe ligand with $Fe(O_2CH)_2$ affords $[Fe_2(BIPhMe)_2(O_2CH)_4]$ [8] which has a (μ-carboxylato-O)bis(μ-carboxylato-O,O') core with five- and six-coordinate iron sites modeling the asymmetry of the deoxyHr core. The bis(μ-carboxylato-O,O') dimetal core found for Mn(II)-reconstituted R2 [2b] and implied for diferrous R2 is modeled by $[Fe_2(OAc)_2(TPA)_2](BPh_4)_2$ [9].

One of the novel spectroscopic properties of the diferrous oxidation state in these proteins is the low field integer spin EPR signal observed at $g \approx 16$ whose intensity is enhanced in parallel mode ($H_\parallel \| H$). Such a signal has been observed for deoxyHrN$_3$ [6], diferrous R2 [10] and reduced MMO [11] and ascribed to ferromagnetically coupled diiron(II) sites. In models, such signals have thus far been observed only for complexes with phenoxo or monodentate carboxylato bridges, e.g. $[Fe^{II}_2(BPMP)(O_2CC_2H_5)_2](BPh_4)$ which has a (μ-phenoxo)bis(μ-carboxylato)diiron core [12], $[Fe^{II}_2(BIPhMe)_2(HCO_2)_4]$ which has a (μ-formato-O)bis(μ-formato-O,O')diiron core [8], and $[Fe^{II}_2(Salmp)_2]^{2-}$ and $[Fe^{II}_2(H_2Hbab)_2(N\text{-MeIm})_2]$ which have bis(μ-phen-

---

*Author to whom correspondence should be addressed.

**Abbreviations used: BIPhMe, 2,2'-bis(1-methylimidazolyl)-phenylmethoxymethane; BPMP, 2,6-bis(bis(2-pyridylmethyl)-aminomethyl)-4-methylphenolate(1 −); HB(3,5-iPr$_2$pz)$_3$, hydro-tris(3,5-diisopropyl-1-pyrazolyl)borate; H$_2$BME-DACO, N,N'-bis(mercaptoethyl)-1,5-diazacyclooctane; H$_4$Hbab, 1,2-bis(2-hydroxybenzamido)benzene; N-MeIm, N-methylimidazole; Me$_3$-TACN, 1,4,7-trimethyl-1,4,7-triazacyclononane; OAc, acetate; OBz, benzoate; Salmp, 2-(bis(salicylideneamino)methyl)pheno-late(3 −); TLA, tris(6-methyl-2-pyridylmethyl)amine; tmen, N,N,N',N'-tetramethylethylenediamine; TMPzA, tris(3,5-dime-thyl-1-pyrazolylmethyl)amine; TPA, tris(2-pyridylmethyl)amine; Tthd, 11,23-dimethyl-3,7,15,19-tetraazotricyclo[19.3.1.1^{9,13}]hexa-cosa-2,7,9,11,13(26),14,19,21(25),22,24-decane-25,26-diol.

oxo)diiron cores [13]. Of these complexes, only for [Fe^{II}$_2$(BPMP)(O$_2$CC$_2$H$_5$)$_2$](BPh$_4$) has a detailed parallel mode EPR study with spectral simulation been reported [12]. In this paper we report the structures and properties of three bis(μ-halo)diiron(II) complexes that exhibit such integer spin EPR signals.

Experimental

Syntheses

Tris(3,5-dimethyl-1-pyrazolylmethyl)amine (TMPzA) [14], tris(2-pyridylmethyl)amine (TPA) [15] and tris(6-methyl-2-pyridylmethyl)amine (TLA) [16] were synthesized according to literature procedures. The syntheses of the metal complexes were all carried out under an argon atmosphere.

[Fe$_2$(TLA)$_2$F$_2$](BF$_4$)$_2$ (1)

A 10 ml methanol solution of TLA (0.33 g, 1 mmol) was added to Fe(BF$_4$)$_2$·6H$_2$O (0.34 g, 1 mmol). Stirring the resulting yellow solution for about 15 min afforded a light yellow powder, which was filtered, washed with methanol, and vacuum dried. Recrystallization of the complex from acetone/ether gave crystals suitable for X-ray single crystal structural determination. *Anal*. Calc. for C$_{42}$H$_{48}$B$_2$F$_{10}$Fe$_2$N$_8$: C, 51.05; H, 4.90; N, 11.34. Found: C, 51.30; H, 4.92; N, 11.56%.

[Fe$_2$(TMPzA)$_2$Cl$_2$](BPh$_4$)$_2$ (2)

A 15 ml methanol solution of TMPzA (0.34 g, 1 mmol) was added to FeCl$_2$·2H$_2$O (0.17 g, 1 mmol) and stirred for 15 min. A 10 ml methanol solution of NaBPh$_4$ (0.34 g, 1 mmol) was added to form white microcrystals, which were filtered, washed with methanol, and vacuum dried. Recrystallization of the complex from acetone/ether gave crystals suitable for X-ray single crystal structural determination. *Anal*. Calc. for C$_{84}$H$_{94}$B$_2$Cl$_2$Fe$_2$N$_{14}$: C, 67.08; H, 6.30; N, 13.04. Found: C, 67.16; H, 6.45; N, 13.12%.

[Fe$_2$(TPA)$_2$Cl$_2$](BPh$_4$)$_2$ (3)

A 10 ml methanolic solution of TPA·3HClO$_4$ (0.40 g, 0.68 mmol) and 3.0 equiv. of trimethylamine (0.21 g, 2.0 mmol) was added to 1 equiv. of FeCl$_2$·2H$_2$O (0.11 g, 0.68 mmol). The resulting yellow solution was stirred for 15 min under argon. Metathesis with NaBPh$_4$ (0.31 g, 0.68 mmol) afforded a yellow powder, which was recrystallized by CH$_3$CN/Et$_2$O. *Anal*. Calc. for

TABLE 1. Crystallographic experiments and computations[a] for 1, 2 and 3

	1 (TLA)	2 (TMPzA)	3 (TPA)
Formula	C$_{42}$H$_{48}$B$_2$F$_{10}$Fe$_2$N$_8$	C$_{84}$H$_{94}$B$_2$Cl$_2$Fe$_2$N$_{14}$	C$_{84}$H$_{76}$B$_2$Cl$_2$Fe$_2$N$_8$
Formula weight (amu)	988.20	1503.98	1401.8
Temperature (K)	172	172	172
Crystal system	triclinic	triclinic	monoclinic
Space group	$P\bar{1}$ (No. 2)	$P\bar{1}$ (No. 2)	$C2/c$ (No. 15)
a (Å)	8.746(7)	10.440(5)	19.211(6)
b (Å)	11.386(4)	11.610(8)	15.264(9)
c (Å)	12.018(6)	16.98(1)	24.52(2)
α (°)	64.44(3)	77.55(6)	90.00
β (°)	81.54(5)	79.63(5)	105.57(3)
γ (°)	87.90(5)	88.90(5)	90.00
V (Å^3)	1067(2)	1977(4)	6926(4)
Z	1	1	4
ρ_{calc} (g cm^{-3})	1.537	1.263	1.344
Crystal dimensions (mm)	0.50 × 0.50 × 0.50	0.55 × 0.40 × 0.35	0.50 × 0.30 × 0.25
Reaction, Mo Kα, λ (Å)	0.7107	0.7107	0.7107
μ(Mo Kα) (cm^{-1})	7.62	4.85	5.47
$2\theta_{max}$ (°)	51.9	55.9	56.0
No. reflections	4183	9535	8630
No. unique data	3371 ($I > 3\sigma(I)$)	5823 ($I > 2\sigma(I)$)	5504 ($I > 2\sigma(I)$)
No. variables	289	469	443
R[b]	0.046	0.042	0.049
R_w[b]	0.063	0.050	0.053
GOF[c]	1.85	1.21	1.15

[a]The intensity data were processed as described in ref. 17. The net intensity $I = [K(\mathrm{NPI})](C - 2B)$, where $K = 17.8$ (attenuator factor), NPI = ratio of fastest possible scan rate to scan rate for the measurement, C = total count, and B = total background count. The standard deviation in the net intensity is given by $[\sigma(I)]^2 = (k/\mathrm{NPI})^2[C + 4B + (pI)^2]$ where p is a factor used to downweight intense reflections. The observed structure factor amplitude F_o is given by $F_o = (I/\mathrm{Lp})^{1/2}$, where Lp = Lorentz and polarization factors. The $\sigma(I)$s were converted to the estimated errors in the relative structure factors $\sigma(F_o)$ by $\sigma(F_o) = 1/2[\sigma(I)/I]F_o$. [b]$R = (\Sigma||F_o| - |F_c||)/(\Sigma|F_o|)$; $R_w = \{(\Sigma w|F_o - F_c|^2)/(\Sigma w(F_o)^2)\}^{1/2}$. [c]The function minimized was $\Sigma w(|F_o| - |F_c|)^2$, where $w = 1/[\sigma(F_o)]^2$. The unweighted and weighted residuals are defined as $R = [\Sigma|(|F_o| - |F_c|)|]/(\Sigma|F_o|)$ and $R_w = \{[\Sigma w(|F_o| - |F_c|)^2]/[\Sigma w(F_o)^2]\}^{1/2}$. The error is an observation of unit weight (GOF), which is $[\Sigma w(|F_o| - |F_c|)^2/(N_o - N_v)]^{1/2}$, where N_o and N_v are the numbers of observations and variables, respectively.

TABLE 2. Fractional coordinates and B_{eq} for **1**, **2** and **3**

Atom	x	y	z	B_{eq}
1				
Fe1	0.02301(5)	0.04122(4)	0.10802(4)	1.27(3)
F1'	0.1438(2)	0.0186(2)	−0.0527(2)	1.6(1)
N1	0.2492(2)	0.1014(3)	0.1273(2)	1.5(2)
N11	00323(3)	0.2607(3)	−0.0070(2)	1.6(2)
N21	−0.0441(3)	0.0805(2)	0.2692(2)	1.4(2)
N31	0.1250(3)	−0.1501(3)	0.2304(2)	1.7(2)
C11	0.3040(4)	0.2179(4)	0.0126(3)	2.3(2)
C12	0.1773(4)	0.3121(3)	−0.0327(3)	2.0(2)
C13	0.2144(5)	0.4420(4)	−0.1040(4)	2.8(3)
C14	0.0992(5)	0.5245(4)	−0.1577(4)	3.1(3)
C15	−0.0439(5)	0.4740(4)	−0.1329(3)	2.8(3)
C16	−0.0814(4)	0.3423(3)	−0.0547(3)	2.0(2)
C17	−0.2430(4)	0.2877(4)	−0.0198(3)	2.4(2)
C21	0.2361(4)	0.1245(4)	0.2403(3)	2.0(2)
C22	0.0719(4)	0.1280(3)	0.3011(3)	1.5(2)
C23	0.0494(4)	0.1750(3)	0.3906(3)	1.9(2)
C24	−0.0990(4)	0.1723(3)	0.4507(3)	2.1(2)
C25	−0.2189(4)	0.1219(3)	0.4210(3)	1.9(2)
C26	−0.1894(4)	0.0761(3)	0.3301(3)	1.6(2)
C27	−0.3186(4)	0.0216(4)	0.2966(3)	2.3(2)
C31	0.3526(4)	−0.0078(4)	0.1373(3)	2.0(2)
C32	0.2778(4)	−0.1371(4)	0.2286(3)	2.0(2)
C33	0.3662(5)	−0.2379(4)	0.2976(4)	2.9(3)
C34	0.2952(5)	−0.3597(4)	0.3662(4)	3.3(3)
C35	0.1409(5)	−0.3753(4)	0.3658(4)	2.9(3)
C36	0.0556(4)	−0.2687(3)	0.3011(3)	2.2(2)
C37	−0.1163(5)	−0.2805(4)	0.3102(3)	2.6(2)
2				
Fe1	0.61074(4)	0.53267(4)	0.40481(2)	1.49(2)
N1	0.6243(2)	0.4567(2)	0.2889(1)	1.8(1)
N11	0.4661(2)	0.6005(2)	0.2667(1)	1.9(1)
N12	0.4872(2)	0.6430(2)	0.3324(1)	1.9(1)
N21	0.7497(2)	0.3230(2)	0.3666(1)	2.0(1)
N22	0.7354(2)	0.3849(2)	0.4275(1)	2.0(1)
N31	0.7585(2)	0.6312(2)	0.2414(1)	1.9(1)
N32	0.7702(2)	0.6380(2)	0.3192(1)	1.9(1)
Cl1	0.58627(7)	0.60670(6)	0.52614(4)	1.98(3)
C11	0.4950(3)	0.4789(2)	0.2665(2)	2.0(1)
C12	0.3912(4)	0.6609(3)	0.1325(2)	3.4(2)
C13	0.4195(3)	0.6834(3)	0.2107(2)	2.5(2)
C14	0.4102(4)	0.7847(3)	0.2415(2)	2.9(2)
C15	0.4541(3)	0.7559(3)	0.3163(2)	2.3(2)
C16	0.4688(4)	0.8343(3)	0.3734(2)	3.2(2)
C21	0.6486(3)	0.3313(2)	0.3175(2)	2.0(1)
C22	0.8914(4)	0.1778(3)	0.3071(2)	3.7(2)
C23	0.8550(3)	0.2536(3)	0.3675(2)	2.4(2)
C24	0.9116(3)	0.2711(3)	0.4305(2)	2.8(2)
C25	0.8351(3)	0.3531(3)	0.4666(2)	2.3(1)
C26	0.8498(3)	0.3996(3)	0.5398(2)	3.0(2)
C31	0.7309(3)	0.5162(3)	0.2261(2)	2.2(1)
C32	0.7921(5)	0.7481(4)	0.0980(2)	4.1(2)
C33	0.7952(3)	0.7328(3)	0.1868(2)	2.6(2)
C34	0.8317(4)	0.8090(3)	0.2311(2)	3.3(2)
C35	0.8154(3)	0.7470(3)	0.3122(2)	2.3(2)
C36	0.8414(4)	0.7897(3)	0.3849(2)	3.3(2)
3				
Fe1	0.73576(2)	0.15341(3)	0.53369(2)	1.72(1)
Cl1	0.71496(5)	0.30536(5)	0.54807(3)	2.47(3)
N1	0.7516(1)	0.0096(2)	0.5261(1)	1.73(9)

(continued)

TABLE 2. *(continued)*

Atom	x	y	z	B_{eq}
3				
N11	0.8428(1)	0.1281(2)	0.5884(1)	2.0(1)
N21	0.6953(1)	0.1046(2)	0.6019(1)	1.8(1)
N31	0.6333(1)	0.1108(2)	0.4781(1)	2.3(1)
C11	0.8292(2)	−0.0012(2)	0.5303(1)	2.1(1)
C12	0.8713(2)	0.0497(2)	0.5810(1)	1.9(1)
C13	0.9339(2)	0.0189(2)	0.6180(1)	2.5(1)
C14	0.9677(2)	0.0690(3)	0.6647(2)	3.1(1)
C15	0.9376(2)	0.1489(3)	0.6725(1)	3.1(1)
C16	0.8762(2)	0.1762(2)	0.6336(1)	2.4(1)
C21	0.7309(2)	−0.0381(2)	0.5724(1)	2.3(1)
C22	0.7004(2)	0.0179(2)	0.6113(1)	1.7(1)
C23	0.6791(2)	−0.0206(2)	0.6552(1)	2.3(1)
C24	0.6513(2)	0.0316(2)	0.6904(1)	2.7(1)
C25	0.6454(2)	0.1211(2)	0.6806(1)	2.4(1)
C26	0.6678(2)	0.1547(2)	0.6363(1)	2.2(1)
C31	0.7048(2)	−0.0149(2)	0.4698(1)	2.3(1)
C32	0.6316(2)	0.0263(2)	0.4620(1)	2.3(1)
C33	0.5680(2)	−0.0174(2)	0.4391(1)	3.1(1)
C34	0.5034(2)	0.0266(3)	0.4323(2)	3.5(2)
C35	0.5043(2)	0.1136(3)	0.4478(2)	3.4(2)
C36	0.5700(2)	0.1536(2)	0.4711(1)	2.8(1)

$C_{84}H_{76}B_2Cl_2Fe_2N_8$: C, 71.97; H, 5.46; N, 7.99, Cl, 5.06. Found: C, 71.73; H, 5.58; N, 7.90; Cl, 5.31%.

X-ray crystallography

Single crystals of the complexes **1**, **2** and **3** suitable for X-ray crystallographic studies were mounted on glass fibres and coated with a viscous hydrocarbon and cooled to − 100 °C to prevent oxidation. All data were collected on an Enraf-Nonius CAD4 diffractometer with graphite monochromated Mo Kα ($\lambda = 0.71069$ Å) radiation. Cell constants and orientation matrixes for data collection were obtained from a least-squares refinement using the setting angles of 25 carefully centered reflections. The intensities of three representative reflections were measured every 50 min of X-ray exposure time throughout the data collection to ascertain crystal integrity. All data were corrected for empirical absorption and Lorentz and polarization effects. Pertinent crystallographic data and experimental conditions are summarized in Table 1.

Each structure was solved by direct methods. All non-hydrogen atoms were refined anisotropically, and hydrogen atoms were placed in calculated positions, assigned thermal parameters that were 20% greater than the B_{eq} value of the atom to which they were bonded and not refined. Refinement was carried out with full-matrix least-squares on F with scattering factors from ref. 18 and included anomalous dispersion terms. Final position parameters of all the nonhydrogen atoms and selected bond lengths and bond angles are listed in Tables 2 and 3, respectively. The maximum and

TABLE 3. Selected bond lengths (Å) and angles (°) for **1**, **2** and **3**[a]

	1	3	2	
Bond lengths (Å)				
Fe1–μ-X1	1.945(2)	2.396(2)	2.370(2)	Fe1–μ-Cl1
Fe1–μ-X1'	2.173(2)	2.516(2)	2.582(2)	Fe1–μ-Cl1'
Fe1–N1	2.193(3)	2.231(3)	2.305(3)	Fe1–N1 .
Fe1–N11	2.273(3)	2.168(3)	2.155(3)	Fe1–N12
Fe1–N21	2.165(3)	2.157(3)	2.143(3)	Fe1–N22
Fe1–N31	2.276(3)	2.171(3)	2.196(3)	Fe1–N32
Fe1–Fe1'	3.198(3)	3.494(3)	3.563(3)	Fe1–Fe1'
Bond angles (°)				
μ-X1–Fe1–μ-X1'	78.28(9)	89.33(3)	88.06(6)	μ-Cl1–Fe1–μ-Cl1'
Fe1–μ-X–Fe1'	101.72(9)	90.67(3)	91.94(6)	Fe1–μ-Cl–Fe1'
μ-X1–Fe1–N1	164.04(9)	175.47(7)	177.18(7)	μ-Cl1–Fe1–N1
μ-X1–Fe1–N11	103.9(1)	104.46(8)	103.74(8)	μ-Cl1–Fe1–N12
μ-X1–Fe1–N21	115.3(1)	96.40(7)	103.76(9)	μ-Cl1–Fe1–N22
μ-X1–Fe1–N31	101.9(1)	102.90(8)	105.51(8)	μ-Cl1–Fe1–N32
μ-X1'–Fe1–N1	85.8(1)	95.20(7)	89.24(8)	μ-Cl1'–Fe1–N1
N1–Fe1–N11	76.3(1)	75.40(9)	75.4(1)	N1–Fe1–N12
N1–Fe1–N21	80.6(1)	79.07(9)	77.1(1)	N1–Fe1–N32
N1–Fe1–N31	76.6(1)	76.9(1)	77.0(1)	N1–Fe1–N22

[a]e.s.d.s in the least significant digits are given in parentheses.

minimum peaks on the final difference Fourier maps corresponded to 1.16 and −0.71, 0.38 and −0.47, and 0.35 and −0.33 e/Å^3, for **1**, **2** and **3**, respectively.

Physical methods

X-band EPR measurements were performed with a Varian E9 spectrometer equipped with an Oxford liquid helium cryostat. A Varian E-236 bimodal cavity was used to generate the microwave fields parallel and perpendicular to the static field. The magnetic field was calibrated with a gauss meter and the microwave frequency was measured with a counter.

Multifield saturation magnetization data were collected on a Quantum Design SQUID susceptometer and fit as described previously [19]. Polycrystalline samples were ground thoroughly and held in place between the gel cap halves physically to give a powder average magnetization in the applied field. No detectable paramagnetic impurities were seen in the gel caps used. The magnetization data were corrected for diamagnetism using the Pascal's constant for the complex [20]. Theoretical powder average magnetization curves were calculated from the spin Hamiltonian shown in eqn. (1) [19]

$$\mathcal{H} = JS_1 \cdot S_2 + \Sigma[D_i(S_{zi}^2 - 2) + E_i(S_{xi}^2 - S_{yi}^2)$$
$$+ \beta S_i \cdot g_i \cdot B]_{i=1,2} \qquad (1)$$

where S_1 and S_2 are the spin states of ion 1 and 2, J is the isotropic exchange coupling constant, D_i and E_i are the axial and rhombic zero-field splitting parameters, and g_i are the g tensors of the uncoupled sites. The

saturation magnetization data were fit by the simplex method [21] to find the spin Hamiltonian parameters yielding the minimum in the standard quality of fit parameter, χ^2, where $\chi^2 = \Sigma(\text{moment}_{exp} - \text{moment}_{fit})^2$. The final fits of the data were obtained without considering any monomeric $S = 2$ Fe^{II} impurity ($\chi^2 = 17$ for **1**, 10 for **2**, 35 for **3**). The amount of paramagnetism found from the fitting process was used to scale the vertical axes of the plots.

Results and discussion

As part of our efforts to understand diferrous sites of hemerythrin, ribonucleotide reductase and methane monooxygenase, we have synthesized three complexes with Fe$_2$X$_2$ cores and report their structural, magnetic and EPR properties.

Crystallographic studies

The ORTEP plots for complexes **1**, **2** and **3** are shown in Fig. 1. The three complexes all have an Fe$_2$X$_2$ core with an inversion center which requires the two Fe and two X atoms to lie in a strict plane. The two bridging halides bind to each iron unsymmetrically with the one *trans* to the amine nitrogen having the shorter Fe–X distance. Each iron has a distorted octahedral environment. The tetradentate tripodal ligands adopt the expected configuration about the iron with N–Fe–N angles averaging ∼77° to accommodate the five-membered chelate rings.

(a)

(b)

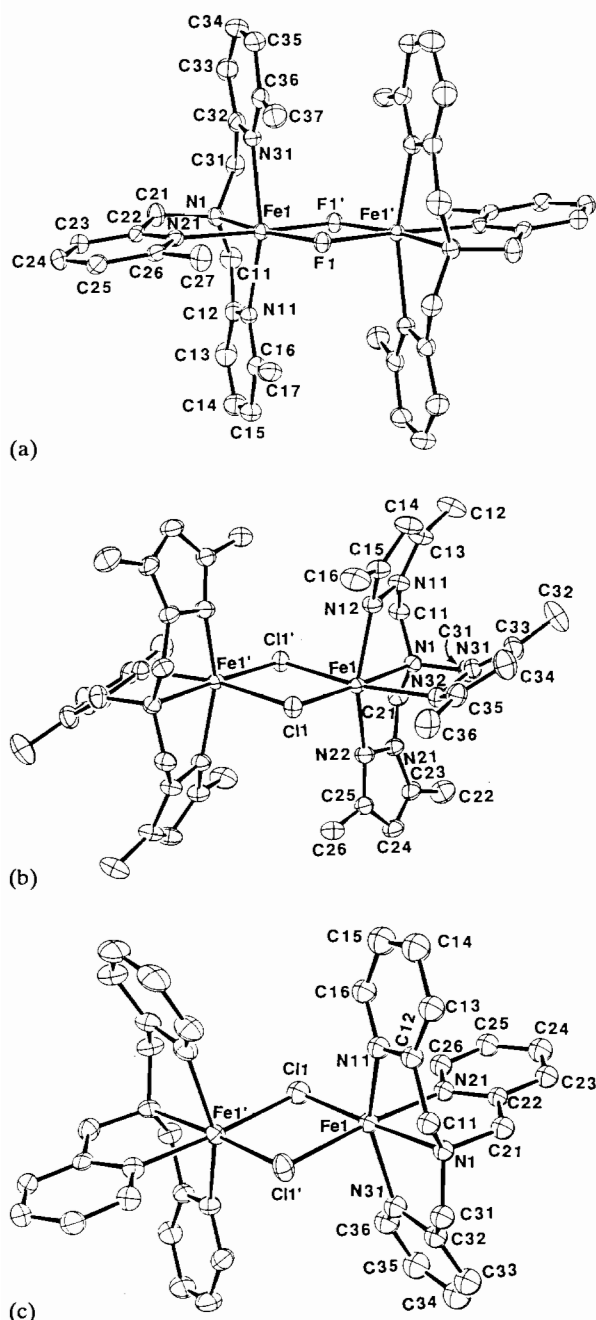(c)

Fig. 1. ORTEP plots of (a): $[Fe_2(TLA)_2F_2]^{2+}$ (**1**), (b) $[Fe_2(TMPzA)_2Cl_2]^{2+}$ (**2**) and (c) $[Fe_2(TPA)_2Cl_2]^{2+}$ (**3**), showing 50% probability ellipsoids. The hydrogen atoms are omitted for clarity.

The structures reflect the differing tripodal ligands and bridge halides. In the case of the TPA and TMPzA complexes, the amine N–Fe bond is longer than the other N–Fe bonds [9], due to the constraints imposed by the tripodal ligand arrangement and typical of other TPA complexes [9, 22]. For **2**, the Fe–N_{amine} bond is 2.305(3) Å long, compared to an average Fe–$N_{aromatic}$ bond of 2.165 Å; for **3**, the Fe–N_{amine} bond is 2.231(3) Å long, compared to an average Fe–$N_{aromatic}$ bond of

2.165 Å. However in the case of **1**, the Fe–N_{amine} bond of 2.193(3) Å is shorter than the average Fe–$N_{aromatic}$ bond of 2.238 Å. This structural difference can be ascribed to the presence of the 6-methyl groups which sterically prevent the two *trans* pyridines from approaching too closely to the metal center. The shorter amine N–Fe bond thus compensates for the weaker aromatic N–Fe bonds in this complex. Other Fe(II)TLA complexes also exhibit this structural feature [23].

The Fe_2X_2 core is perhaps the most interesting feature of these complexes. Complex **1** represents the first example of a bis(μ-fluoro)diiron(II) complex. The Fe–F bond lengths are 1.945(2) and 2.173(2) Å long, comparable to the Fe–μ-O bonds of bis(μ-hydroxo)- [24] and bis(μ-phenoxo)diiron(II) complexes [25] (Table 4). Like these latter complexes, the Fe–Fe distance for **1** is 3.198(3) Å. The Fe–μ-F–Fe angle is 101.72(9)°, which is on the larger end of the range observed for Fe–X–Fe angles in Table 4. The large Fe–X–Fe angle probably results from the steric effect of the TLA methyl groups, especially the C27 methyl group which pushes F1 away. This steric interaction results in a larger N21–Fe–F1 angle (115.3(1)°) and a smaller F1–Fe–F1' angle and in turn the observed larger Fe–F–Fe angle.

Relative to **1**, the core dimensions of **2** and **3** are larger because of the bridging chlorides. The Fe–Cl bonds of **2** and **3** fall within the range of distances observed for this type of bond, and expectedly longer than terminal Fe–Cl bonds [25b, 26, 27]. Due to differences in the *trans* ligands, the Fe–Cl and Fe–Cl' bonds differ in length. The Fe–Cl bonds of **2** and **3** are nearly perpendicular to each other, affording Fe–X–Fe' angles of 91.94(6) and 90.67(3)°, respectively. The Fe–Fe distances for **2** and **3** are 3.563(3) and 3.494(3) Å, respectively, which are shorter than those in other crystallographically characterized diferrous complexes with Fe_2X_2 cores like [(BME-DACO)NiFeCl$_2$]$_2$ (**4**) [26] and [LFeCl$_2$]$_2$ (**5**) (L=2,2'-dithiazolyldisulfide) [27], and [(CH$_3$)$_3$NH]FeCl$_3$·2H$_2$O [28] (**6**), a polymeric material with repeating Fe$_2$Cl$_2$ rhombs.

Magnetization and EPR studies

Magnetization data for polycrystalline samples of **1**, **2** and **3** were collected at four fixed fields ranging from 0.1 to 5.0 T, over the temperature range of 2 to 200 K. Plotted in Fig. 2(a) is the effective magnetic moment of **1** versus temperature where μ_{eff} increases from 7.4 μ_B per complex at room temperature to 8.4 μ_B per complex at 3 K. The rise from horizontal with decreasing temperature graphically indicates ferromagnetic coupling between the two high spin iron(II) centers of **1**. Similar conclusions can be reached for complexes **2** and **3**.

TABLE 4. Comparison of the properties of the diferrous complexes[a]

Property	1	2	3	4	5	6	7	8	9	10	11	12
Fe–Fe (Å)	3.198	3.563	3.494	3.725	3.654	3.680	3.117	3.202	3.165	3.190	3.177	3.179
Fe–μ-X (Å)	1.945	2.370	2.396	2.422	2.295	2.485	2.091	2.129	1.997	2.01	2.021	2.016
	2.173	2.582	2.516	2.547	2.792	2.544	2.092	2.145	2.167	2.06	2.042	2.04
								2.168		2.08		
								2.195		2.22		
Fe–μ-X–Fe (°)	101.72	91.94	90.67	97.1	91.3	95.4	93.3	95.6	98.9	97.7	102.9	103.3
								95.9		100.7		
Coord. no.	6,6	6,6	6,6	5,5	5,5	6,6	6,6	6,6	5,5	6,5	4,4	5,5
J (cm^{-1})	−1.2	−2.6	−10.0	>0	nr	−24.2	3.0	−2.46	~ −5.0	nr[c]	nr	nr
Reference	[b]	[b]	[b]	26	27	28	25a	13a	13b	13b	25b	24

[a] 4 = [(BME-DACO)NiFeCl$_2$]$_2$;   5 = [(L)FeCl$_2$]$_2$,   L = 2,2'-dithiazolyldisulfide;   6 = [(CH$_3$)$_3$NH]FeCl$_3$2H$_2$O;   7 = [Fe(Tthd)Im$_4$]$^{2+}$; 8 = [Fe(salmp)$_2$]$^{2-}$;   9 = [Fe(H$_2$Hbab)$_2$(N-MeIm)$_2$];   10 = [Fe(H$_2$Hbab)$_2$(DMF)$_2$(N-MeIm)];   11 = [Fe$_2$Cl$_4$(o-C$_6$H$_4$-p-CH$_3$)$_2$]$^{2-}$; 12 = [Fe(OH)(HB(3,5-i-Pr$_2$pz)$_3$]$_2$.   [b] This work.   [c] nr = not reported.
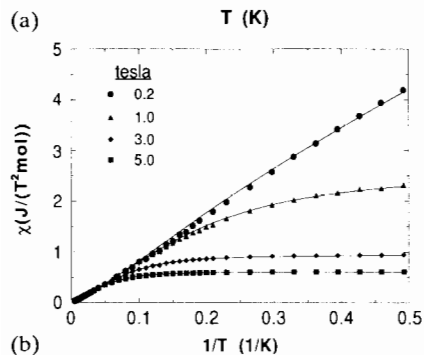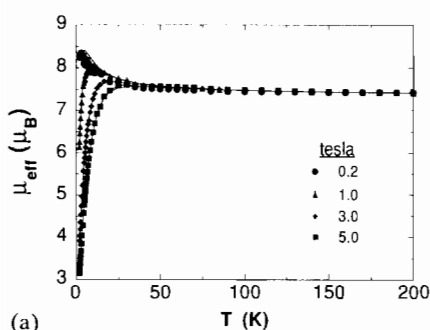

Fig. 2. Magnetization of [Fe$_2$(TLA)$_2$F$_2$](BF$_4$) (1) at four fixed fields over the temperature range 2–200 K. (a) Effective magnetic moment (μ_{eff}) versus temperature are plotted. (b) All four fields plotted as molar susceptibility (χ_{mol}) versus inverse temperature. The solid lines were calculated by diagonalizing the full 25×25 spin Hamiltonian of equation 1, assuming identical ferrous sites having coaxial zero-field splitting tensors with $J = -1.2$ cm^{-1}, $|D_i| = 7.2$ cm^{-1}, $E_i/D_i = 0.11$, and $g_i = 2.12(3)$.

Fig. 3. Magnetization of 2 (a) and 3 (b) at four fields over the temperature range 2–200 K are plotted as molar susceptibility (χ_{mol}) versus inverse temperature. A least-squares fit to the data found $J = -2.6(2)$ cm^{-1}, $|D_i| = 7.2(5)$ cm^{-1}, $E_i/D_i = 0.27(3)$ and $g_i = 2.15(3)$ for 2, and $J = -10.0(2)$ cm^{-1}, $|D_i| = 13.2(5)$ cm^{-1}, $E_i/D_i = 0.17(3)$ and $g_i = 2.15(3)$ for 3.

The three data sets are plotted as molar susceptibility (χ_{mol}) versus inverse temperature at the four fields in Figs. 2(b) and 3. Note that the magnetic susceptibilities of all three complexes at the lowest field are the largest at lower temperatures (relative to those of other fields at these temperatures). This is also indicative of ferromagnetic coupling [6b]. Fits to the multifield saturation magnetization curves allow the extent of ferromagnetic coupling and the zero field splitting
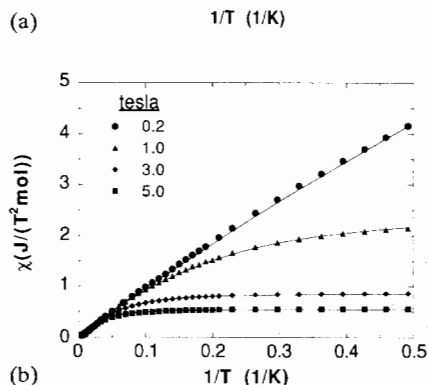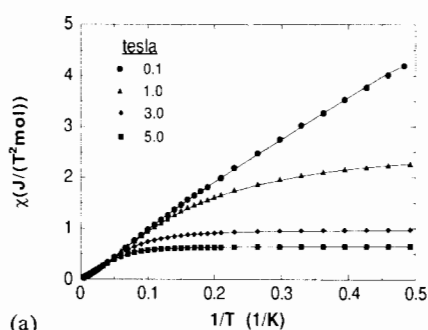
parameters to be deduced. The solid lines are least-squares fits calculated by diagonalization of the 25×25 matrix representation for the spin Hamiltonian of eqn. (1) under the assumption of equal and coaxial D_i tensors and isotropic $g_1 = g_2 = g_i$. The final parameter set of the best fit for 1: $J = -1.2(2)$ cm^{-1}, $|D_i| = 7.2(5)$ cm^{-1}, $g_i = 2.12(3)$; for 2: $J = -2.6(2)$ cm^{-1}, $|D_i| = 7.2(5)$ cm^{-1}, $g_i = 2.15(3)$; for 3: $J = -10.0(2)$ cm^{-1}, $|D_i| = 13.2(5)$ cm^{-1}, $g_i = 2.15(3)$. Thus 1 and 2 show weak ferromagnetic
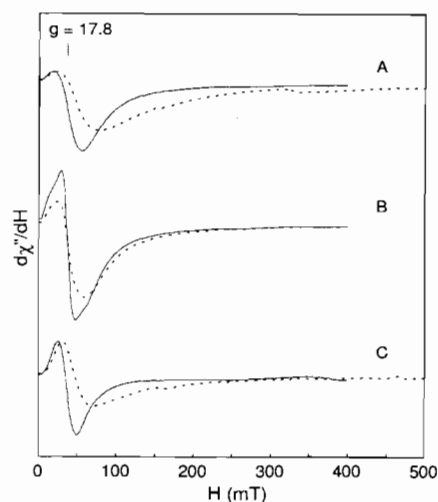
Fig. 4. X-band EPR spectra of solid (A) **1**, (B) **2** and (C) **3** at 3 K. The microwave field orientation is $H_1 \| H$ (——) and $H_1 \perp H$ (– – –). Instrumental parameters: microwaves, 0.2 mW at 9.1 GHz; modulation, 1 mTpp at 100 kHz.

coupling, whereas **3** exhibits stronger ferromagnetic coupling.

Complexes **1–3** exhibit low field EPR signals near $g = 18$ as shown in Fig. 4. The signals grow in intensity and sharpen for $H_1 \| H$ as is characteristic of integer spin doublets [29]. The temperature dependence of the signals indicates that the $g \approx 18$ resonances from all three complexes originate from ground spin doublets. As demonstrated in previous work [6b], a ground spin doublet will have a resonance near $g = 16$ for ferromagnetically coupled Fe(II) sites, thus corroborating the magnetic susceptibility fits with $J < 0$.

Perspective

With complexes **1–3**, we have augmented the number of diferrous Fe_2X_2 complexes and characterized their magnetic and EPR properties. Like $[Fe_2(salmp)_2]^{2-}$ [13a], the complexes are ferromagnetically coupled and exhibit integer spin EPR signals. These properties undoubtedly arise from the acute Fe–X–Fe angles imposed by the Fe_2X_2 rhomb. Complex **3** has the Fe–X–Fe angle closest to 90° among these complexes and, perhaps not surprisingly, exhibits the largest ferromagnetic coupling. However complex **2** has an Fe–X–Fe angle only 1° larger and J diminishes almost fourfold. It is thus premature at this stage to draw generalities since the database for such complexes is quite small.

The Fe_2X_2 complexes discussed above exhibit EPR properties very similar to those reported for the diferrous states of the diiron–oxo proteins, particularly deoxy-hemerythrin azide [6] and reduced methane monooxygenase [11]. While a bis(μ-halo)diferrous structure can

probably be excluded from consideration, other similarly bridged structures may give rise to $g \approx 16$ integer spin EPR signals and should be considered as possible structures for the proteins whose active sites are, at present, poorly defined.

Supplementary material

The following are available on request from the authors: Table Suppl. 1: bond lengths and bond angles for **1** (6 pages), **2** (8 pages) and **3** (7 pages); Table Suppl. 2: position parameters and B_{eq} of all atoms for **1** (3 pages), **2** (4 pages) and **3** (4 pages). Table Suppl. 3: thermal parameters of all atoms for **1** (4 pages), **2** (6 pages) and **3** (5 pages).

Acknowledgements

References

1 (a) M.A. Holmes, I.L. Trong, S. Turley, L.C. Sieker and R.E. Stenkamp, *J. Mol. Biol., 218* (1991) 583–593; (b) S. Sheriff, W.A. Hendrickson and J.L. Smith, *J. Mol. Biol., 197* (1987) 273; (c) R.E. Stenkamp, L.C. Sieker, L.H. Jensen, J.D. McCallum and J. Sanders-Loehr, *Proc. Natl. Acad. Sci. USA, 82* (1985) 713.

2 (a) P. Norlund, B.-M. Sjöberg and H. Eklund, *Nature (London), 345* (1990) 593; (b) M. Atta, P. Nordlund, A. Årberg, H. Eklund and M. Fontecave, *J. Biol. Chem., 267* (1992) 20682.

3 (a) B.G. Fox, W.A. Froland, J.E. Dege and J.D. Lipscomb, *J. Biol. Chem., 264* (1989) 10023; (b) J.G. DeWitt, J.G. Bensten, A.C. Rosenzweig, B. Hedman, J. Green, S. Pilkington, G.C. Papaefthymiou, H. Dalton, K.O. Hodgson and S.J. Lippard, *J. Am. Chem. Soc. 113* (1991) 9219.

4 L. Que, Jr. and A.E. True, *Prog. Inorg. Chem., 38* (1990) 97.

5 (a) P. Chaudhuri, K. Wieghardt, B. Nuber and J. Weiss, *Angew. Chem., Int. Ed. Engl., 24* (1985) 778; (b) J.R. Hartman, R.L. Rardin, P. Chaudhuri, K. Pohl, K. Wieghardt, B. Nuber, J. Weiss, G.C. Papaefthymiou, R.B. Frankel and S.J. Lippard, *J. Am. Chem. Soc., 109* (1987) 7387.

6 (a) R.C. Reem and E.I. Solomon, *J. Am. Chem. Soc., 109* (1987) 1216; (b) M.P. Hendrich, L.L. Pearce, L. Que, Jr., N.D. Chasten and E.P. Day, *J. Am. Chem. Soc., 113* (1991) 3039.

7 K.S. Hagen and R. Lachicotte, *J. Am. Chem. Soc., 114* (1992) 8741.

8 (a) W.B. Tolman, A. Bino and S.J. Lippard, *J. Am. Chem. Soc., 111* (1989) 8522; (b) W.B. Tolman, S. Liu, J.G. Bensten and S.J. Lippard, *J. Am. Chem. Soc., 113* (1991) 152.

9 S. Ménage, Y. Zang, M.P. Hendrich and L. Que, Jr., *J. Am. Chem. Soc., 114* (1992) 7786.

48

10 (a) J.B. Lynch, C. Juarez-Garcia, E. Münck and L. Que, Jr., *J. Biol. Chem. 264* (1989) 8091; (b) T.E. Elgren, M.P. Hendrich and L. Que, Jr., submitted for publication.

11 M.P. Hendrich, E. Münck, B.G. Fox and J.D. Lipscomb, *J. Am. Chem. Soc., 112* (1990) 5861.

12 A.S. Borovik, M.P. Hendrich, T.R. Holman, E. Münck, V. Papaefthymiou and L. Que, Jr., *J. Am. Chem. Soc., 112* (1990) 6031.

13 (a) B.S. Snyder, G.S. Patterson, A.J. Abrahamson and R.H. Holm, *J. Am. Chem. Soc., 111* (1989) 5214; (b) A. Stassinopoulos, G. Schulte, G.C. Papaefthymiou and J.P. Caradonna, *J. Am. Chem. Soc., 113* (1991) 8686.

14 W.L. Drissen, R.A.G. De Graaff, J. Ochocki and J. Reedijk, *Inorg. Chim. Acta, 150* (1988) 41.

15 B.G. Gafford and R.A. Holwerda, *Inorg. Chem., 28* (1989) 60.

16 M.M. De Mota, J. Rodgers and S.M. Nelson, *J. Chem. Soc. A*, (1969) 2036.

17 *CAD4 and SDP-PLUS User's Manual*, B.A. Frenz & Assoc., College Station, TX, USA, 1982.

18 *International Tables for X-ray Crystallography*, Vol. IV, Kynoch, Birmingham, UK, 1974, Table 2.2 A.

19 E.P. Day, T.A. Kent, P.A. Lindahl, E. Münck, W.H. Orme-Johnson, H. Roder and A. Roy, *Biophys. J., 52* (1987) 837.

20 E.A. Boudreaux, L.N. Mulay, *Theory and Applications of Molecular Paramagnetism*, Wiley, New York, 1976.

21 J. Nelder and R. Mead, *Comput. J.,* (1965) 308.

22 (a) H.G. Jang, D.D. Cox and L. Que, Jr., *J. Am. Chem. Soc., 113* (1991) 9200; (b) R.E. Norman, S. Yan, L. Que, Jr., G. Backes, J. Ling, J. Sanders-Loehr, J.H. Zhang and C.J. O'Connor, *J. Am. Chem. Soc., 112* (1990) 1554.

23 (a) Y. Chiou and L. Que, Jr., *J. Am. Chem. Soc., 114* (1992) 7567; (b) Y. Zang, T.E. Elgren, Y. Dong and L. Que, Jr., *J. Am. Chem. Soc., 115* (1993) 811.

24 N. Kitajima, N. Tamura, M. Tanaka and Y. Moro-oka, *Inorg. Chem., 31* (1992) 3342.

25 (a) C.L. Spiro, S.L. Lambert, T.J. Smith, E.N. Duesler, R.R. Gagne and D.N. Hendrickson, *Inorg. Chem., 20* (1981) 1229; (b) D. Coucouvanis, K. Greiwe, A. Salifoglou, P. Challen, A. Simopoulos and A. Kostikas, *Inorg. Chem., 27* (1988) 594.

26 D.K. Mills, Y.M. Hsiao, P.J. Farmer, E.V. Atnip, J.H. Reibenspies and M.Y. Darensbourg, *J. Am. Chem. Soc., 113* (1991) 1421.

27 E.S. Raper, A. Miller, T. Glowiak and M. Kubiak, *Transition Met. Chem., 14* (1989) 319.

28 R.E. Greeney, C.P. Landee, J.H. Zhang and W.M. Reiff, *Phys. Rev. B, 39* (1989) 12200.

29 M.P. Hendrich and P.G. Debrunner, *Biophys. J., 56* (1989) 489.